

Research Article

Single-cell RNA-seq and bulk-seq identify RAB17 as a potential regulator of angiogenesis by human dermal microvascular endothelial cells in diabetic foot ulcers

Hengyu Du^{1,†}, Shenghong Li^{1,†}, Jinqiang Lu¹, Lingzhi Tang¹, Xiao Jiang¹, Xi He¹, Jiaji Liang¹, Xuan Liao¹, Taixing Cui^{2,*}, Yuesheng Huang^{3,*} and Hongwei Liu^{1,*}

¹Department of Plastic Surgery of the First Affiliated Hospital of Jinan University, Institute of New Technology of Plastic Surgery of Jinan University, Key Laboratory of Regenerative Medicine of Ministry of Education, Guangzhou 510630, P.R. China, ²Dalton Cardiovascular Research Center, Department of Medical Pharmacology and Physiology, University of Missouri, School of Medicine, 134 Research Park Dr, Columbia, MO 65211, USA and ³Institute of Wound Repair and Regeneration Medicine, Southern University of Science and Technology School of Medicine, and Department of Wound Repair, Southern University of Science and Technology Hospital, Shenzhen, Guangdong, 518055, China

*Correspondence. Taixing Cui, Email: taixingcui@health.missouri.edu; Yuesheng Huang, Email:yshuang1958@163.com; Hongwei Liu, Email:liuhongwei0521@hotmail.com

[†]Hengyu Du and Shenghong Li contributed equally to this work.

Received 17 September 2022; Revised 10 January 2023; Accepted 22 March 2023

Abstract

Background: Angiogenesis is crucial in diabetic wound healing and is often impaired in diabetic foot ulcers (DFUs). Human dermal microvascular endothelial cells (HDMECs) are vital components in dermal angiogenesis; however, their functional and transcriptomic characteristics in DFU patients are not well understood. This study aimed to comprehensively analyse HDMECs from DFU patients and healthy controls and find the potential regulator of angiogenesis in DFUs.

Methods: HDMECs were isolated from skin specimens of DFU patients and healthy controls via magnetic-activated cell sorting. The proliferation, migration and tube-formation abilities of the cells were then compared between the experimental groups. Both bulk RNA sequencing (bulk-seq) and single-cell RNA-seq (scRNA-seq) were used to identify RAB17 as a potential marker of angiogenesis, which was further confirmed via weighted gene co-expression network analysis (WGCNA) and least absolute shrink and selection operator (LASSO) regression. The role of RAB17 in angiogenesis was examined through *in vitro* and *in vivo* experiments.

Results: The isolated HDMECs displayed typical markers of endothelial cells. HDMECs isolated from DFU patients showed considerably impaired tube formation, rather than proliferation or migration, compared to those from healthy controls. Gene set enrichment analysis (GSEA), fGSEA, and gene set variation analysis (GSVA) of bulk-seq and scRNA-seq indicated that angiogenesis was downregulated in DFU-HDMECs. LASSO regression identified two genes, *RAB17* and *CD200*, as characteristic of DFU-HDMECs; additionally, the expression of RAB17 was found to be significantly reduced in DFU-HDMECs compared to that in the HDMECs of healthy controls. Overexpression of RAB17 was found to enhance angiogenesis, the expression of hypoxia inducible factor-1α

© The Author(s) 2023. Published by Oxford University Press.

and vascular endothelial growth factor A, and diabetic wound healing, partially through the mitogen-activated protein kinase/extracellular signal-regulated kinase signalling pathway.

Conclusions: Our findings suggest that the impaired angiogenic capacity in DFUs may be related to the dysregulated expression of RAB17 in HDMECs. The identification of RAB17 as a potential molecular target provides a potential avenue for the treatment of impaired angiogenesis in DFUs.

Key words: Human dermal microvascular endothelial cells, Angiogenesis, Diabetic foot ulcers, RAB17, Single-cell RNA-seq, Diabetic wound healing

Highlights

- DFU-HDMECs showed impaired tube formation, rather than proliferation or migration.
- Integrated bulk-seq and scRNA-seq analysis showed significant negative enrichment of angiogenesis in DFU-HDMECs.
- WGCNA and LASSO regression identified RAB17 as a potential marker of angiogenesis.
- Overexpression of RAB17 rescued diabetes-induced impairment of angiogenesis *in vitro* and *in vivo* through mitogen-activated protein kinase/extracellular signal-regulated kinase signalling.

Background

Diabetic foot ulcers (DFUs) are the major cause of limb amputations among patients with diabetes, affecting $\sim 25\%$ of the population [1]. Although several effective measures exist to regulate wound-site pressure, immune response, glycaemic levels, neuronal function and vascular problems [2], the issue of impaired angiogenesis persists [3,4]. Angiogenesis, the process of formation of new blood vessels from preexisting vessels, is crucial for wound healing, as it maintains oxygen and nutrient supply at the wound site [5,6]. Proand anti-angiogenic factors, including chemokines, angiopoietins, endogenous inhibitors, junctional molecules, integrins and oxygen-sensing agents, tightly regulate angiogenesis [7]. Numerous topical and systemic therapies aimed at improving angiogenesis have been developed; however, few have been effective in treating diabetic wounds [8]. Although much research has focused on pro- and anti-angiogenic factors, limited studies have directly assessed DFU-derived endothelial cells (ECs).

Human dermal microvascular ECs (HDMECs), which are the primary ECs in human skin, have been widely used to study angiogenesis in various skin conditions such as scleroderma [9], angioedema [10] and psoriasis [11]. However, their use in studying angiogenesis in DFUs has been limited. Through experimental comparisons of microvessel- and large blood vessel-derived ECs, previous studies have demonstrated that HDMECs and human umbilical vein endothelial cells (HUVECs) differ in their intrinsic angiogenic capacities and levels of tight junctions [12,13]. Additionally, the transcriptome of ECs derived from the large vessels of diabetic patients has also been shown to differ from that of HUVECs exposed to high glucose levels *in vitro* [14]. Therefore, it is expected that DFU-derived HDMECs would be more closely related to human skin ECs under this specific disease state as

opposed to their *in vitro* counterparts. However, it remains unclear whether and how the functional and transcriptional characteristics of DFU patient-derived HDMECs differ from those of healthy HDMECs.

According to the Matrigel tube-formation assay, the endothelial function of ECs was impaired under hyperglycaemic conditions in vitro [15]. Despite endothelial dysfunction, diabetes-impaired angiogenesis is associated with the unstable activity of hypoxia inducible factor- 1α (HIF-1α) [16] and downregulated expression of vascular endothelial growth factor (VEGF, mainly VEGF-A) [17]. However, it remains unclear whether these factors are expressed differently in DFU patient-derived HDMECs. Recently, RAB17, a small GTPase, was found to regulate the formation of tumour neo-vasculature in hepatocellular carcinoma and non-small cell lung cancer [18,19], possibly by regulating HIF-1 α and VEGF-A expression [19]. RAB17 was also reported to participate in cell polarization [20], which is an essential stage in tube formation. Consequently, we hypothesised that RAB17 contributes to the impairment of the angiogenic function of HDMECs, thus affecting diabetic wound healing.

In this study, we conducted a comprehensive analysis of HDMECs derived from DFU patients and healthy controls and compared their phenotypes (including proliferation, migration and tube formation). An integrated analysis of bulk RNA sequencing (bulk-seq) and single-cell RNA sequencing (scRNA-seq) was applied to find the potential regulator of angiogenesis in DFUs. Furthermore, we performed *in vitro* and *in vivo* biochemical analyses to understand the role of RAB17 in diabetic wound healing. Our findings would help in developing strategies for restoring impaired angiogenesis in DFUs and promoting diabetic wound healing.

Methods

Patients

DFU patients and healthy subjects without diabetes mellitus were recruited from the First Affiliated Hospital of Jinan University in Guangzhou, China. Skin specimens were surgically collected from the feet of patients for HDMEC isolation. The study adhered to the principles outlined in the Declaration of Helsinki and was approved by the Medical Ethics Committee of the First Affiliated Hospital of Jinan University. All participants provided written informed consent and those with co-morbidities that could affect the DFU healing were excluded. Detailed clinical characteristics of the participants are presented in Table S1, see online supplementary material.

Diabetic mouse wound-healing model and adeno-associated virus vector administration

The Laboratory Animal Ethics Committee of Jinan University approved the animal experimental protocol. In this study, 4–6 week old C57BL/6 J mice, obtained from the Guangdong Medical Laboratory Animal Center, were utilized. The diabetic wound-healing model in mice was induced as described previously [15]. Streptozotocin (STZ) was intraperitoneally administered to the mice at a dose of 50 mg/kg for 5 days. Blood glucose levels were measured 1 week after STZ injection using a blood glucose monitor (Roche, Basel, Switzerland). Mice with fasting blood glucose level >250 mg/dl were considered diabetic. The mice were randomly allocated into two groups. Full-thickness skin wounds (8 mm in diameter) were created using a biopsy punch 4 weeks after STZ injection.

The RAB17-overexpressing recombinant adeno-associated viral (rAAV) vector was constructed and synthesized by WZBio (Jinan, Shandong, China). Each viral suspension, containing 5×10^{10} vector genomes of either rAAV-RAB17 or rAAV-vector, was suspended in 50 μ l of normal saline and intradermally injected into the backs of mice 3 weeks before wound creation, using a 31-gauge needle. Two weeks after AAV injection, western blot and immunohistochemistry were performed to confirm RAB17 overexpression in mouse skin. Digital images of wounds were photographed at the indicated times. Wound area was analysed using ImageJ software (http://imagej.nih.gov/ij, National Institutes of Health (NIH), USA). Wound blood perfusion was determined with the laser speckle contrast imager (FLPI-2, Moor Instruments).

Cell cultures

Fresh skin samples were obtained and kept in PBS on ice according to the manufacturer's instructions before being transferred to the laboratory. After the removal of necrotic tissues, the remaining non-necrotic tissues were minced and digested with 2.4 units/ml of dispase (Roche, Basel, Switzerland) and 0.25% type I collagenase (Sigma-Aldrich, St. Louis, MO, USA) at 37°C for 2 h. The resulting cell suspensions were collected and filtered through a 40- μ m strainer, followed by culturing in EBM-2 MV medium with growth factors

and 5% fetal bovine serum (FBS; Lonza, Basel, Switzerland) for the isolation of HDMECs via magnetic-activated cell sorting (MACS) using a CD31 MicroBead Kit (Miltenyi Biotech, San Diego, CA, USA). HDMECs were cultured on 1% gelatin-coated plates and expanded for 5 days, followed by re-purification to improve purity. Human umbilical artery smooth muscle cells (HUASMCs, negative control cells) were donated by Dr Xiaomin Xiao and cultured in Dulbecco's modified Eagle's medium-F12 supplemented with 5% FBS (Thermo Fisher Scientific, Waltham, MA, USA). Cells isolated between passages 3 to 6 were used for experimental analysis.

For incubation of HDMECs in high glucose, healthy HDMECs [normal (Nor)-HDMECs] were incubated in high-glucose medium (30 mM D-glucose) for 2 and 7 days, while culture medium containing 30 mM mannitol served as an osmotic control [21].

Flow cytometry

HDMECs and fibroblasts were collected and washed, and incubated with phycoerythrin-cyanine7 anti-human CD31 (Invitrogen, Waltham, MA, USA) and allophycocyanin anti-human CDH5 (Biolegend, San Diego, CA, USA) antibodies at 1:20, along with their corresponding isotype control antibodies for 30 min at 4°C following the manufacturers' instructions. Fibroblasts were employed as the negative control. Flow cytometry assay was performed on an LSR II (BD Bioscience, San Diego, CA, USA). Data analysis was conducted using FlowJo (FlowJo, Ashland, OR, USA). Gating strategies are outlined in Figure S1, see online supplementary material.

Immunofluorescence

Cells were fixed with 4% paraformaldehyde for 15 min at room temperature, followed by blocking and incubation with diluted primary antibodies against CDH5 (R&D systems, Minneapolis, MN, USA), CD31, von Willebrand Factor (vWF) and actin alpha 2 smooth muscle (α -SMA) (Abcam, Cambridge, UK) at 4°C overnight. The cells were then washed and incubated with secondary antibodies, either goat antimouse IgG (H+L) fluor594-conjugated secondary antibody or goat anti-rabbit IgG (H+L) fluorescein isothiocyanateconjugated secondary antibody (Affinity, Jiangsu, China), according to the corresponding species of the primary antibodies for 1 h at room temperature. The nuclei were stained with 4',6-diamidino2-phenylindole (DAPI; Invitrogen, Waltham, MA, USA). Fluorescent images were captured using a LAS X microscope (Leica Microsystems, Heerbrugg, St. Gallen, Switzerland).

RNA isolation and quantitative real-time PCR

Total RNA was isolated using an RNAprep pure Cell/Bacteria Kit (Tiangen, Beijing, Beijing, China). The resulting cDNA was prepared using a ReverTra Ace qPCR RT Kit (TOYOBO, Osaka, Osaka Prefecture, Japan). Quantitative realtime PCR (qPCR) was conducted using the Bio-Rad CFX Connect system using SYBR® Green Realtime PCR Master

Mix (TOYOBO, Osaka, Osaka Prefecture, Japan) according to the manufacturer's protocols. Primer sequences of target genes are listed in Table S2, see online supplementary material.

Western blotting

Cells lysis was conducted using RIPA buffer, supplemented with a protease inhibitor cocktail (Roche, Basel, Kanton Basel, Switzerland). Protein samples of 20 µg were separated through sodium dodecyl sulphate-polyacrylamide gel electrophoresis gels with either 8 or 12% concentrations. These samples were then wet-transferred onto polyvinylidene fluoride membranes (Millipore, Burlington, MA, USA). Membranes were subsequently blocked and incubated with diluted primary antibodies: anti- β -actin antibody (1 : 2000, Servicebio, Wuhan, Hubei, China), anti-CD31 antibody (1:500, Novus, Minneapolis, MN, USA), anti-CDH5 antibody (1: 500, R&D systems, Minneapolis, MN, USA), anti-α-SMA antibody (1: 3000, Abcam, Cambridge, UK), anti-RAB17 and anti-HIF-1α antibodies (1 : 1000, Zenbio, Chengdu, China), anti-VEGF-A, anti-extracellular signal-regulated kinase (ERK)1/2 and anti-phospho-ERK1/2 antibodies (1: 1000, Zenbio, Chengdu, China), anti-Akt and anti-Phospho-Akt antibodies (1: 500, Zenbio, Chengdu, China) at 4°C overnight. Membranes were washed three times and incubated with the corresponding secondary antibodies. The protein signals were detected using the enhanced chemiluminescence reagent (Beyotime, Shanghai, China) on a Tanon 5200 chemiluminescent imaging system (Tanon, Shanghai, China) and band intensities were measured using ImageJ.

Cell proliferation assays

Ninety-six-well plates were coated with 1% gelatin for 30 min at 37°C. HDMECs were then serum-starved overnight in EBM-2 medium supplemented with 0.2% FBS. Subsequently, a seeding density of 0.2 × 10⁴ cells/well was introduced onto the plates with full EBM-2 MV medium (Lonza, Basel, Kanton Basel, Switzerland). The initiation of cell seeding was considered as the zero-time point (0 h). At predetermined intervals of 24, 48, 72, 96 and 120 h of incubation, cells were trypsinized, collected and quantified utilizing a Scepter automatic cell counter (Millipore, Burlington, MA, USA).

5-Ethynyl-2'-deoxyuridine (EdU) proliferation assays

EdU proliferation assay was performed using the Cell-Light EdU Apollo 567 In Vitro Kit (Ribo Bio, Guangzhou, Guangdong, China) according to the manufacturer's instructions. HDMECs were seeded in triplicate on 1% gelatin-coated 48-well plates at 5×10^4 cells/ml and cultured under standard conditions for 48 h. Thereafter, cells were cultured with fresh medium containing 50 μ M EdU for 4 h before fixation, neutralization, permeabilization and Apollo staining. Cell nuclei were subsequently stained with Hoechst 33342. Fluorescent

images were captured using LAS X. The ratio of EdU-positive cells was then analyzed using ImageJ.

Wound scratch assays

To evaluate the migration ability of HDMECs, the cells were serum-starved overnight in EBM-2 medium supplemented with 0.2% FBS. Then, HDMECs were seeded in triplicate at 2×10^4 cells/well into a Culture-Insert 2 Well (ibidi, Gräfelfing, BY, Germany), which was placed on 1% gelatin-coated 6-well plates. The Culture-Insert was removed after cell attachment, thereby creating a cell-free gap. Pictures were captured at 0 and 24 h after the creation of the scratch using LAS X. Wound areas were calculated by ImageJ. Wound closure rate was calculated by dividing the wound area at 24 h by the wound area at 0 h.

Transwell assays

HDMECs were serum-starved overnight prior to the transwell assay. After trypsinization, cells were cultured in triplicate at 2×10^4 cells/well in the upper compartments of the transwell chambers with 8.0 μ m pores (Corning, Corning, NY, USA) in EBM-2 medium containing 0.1% FBS. The lower chambers were filled with the EBM-2 MV medium. Following a 24 h incubation period, cells were fixed by 4% paraformaldehyde and the cells on the inner membrane were swept with a cotton swab. Cells that migrated to the outer membrane were stained for 30 min in 0.1% crystal violet solution. Five different fields were photographed using LAS X. ImageJ was used to calculate the average sum of migrated cells.

Matrigel tube-formation assays

Ninety-six well plates were coated with Matrigel® Growth Factor Reduced Basement Membrane Matrix (Corning, Corning, NY, USA) for 30 min prior to cell planting. After trypsinization, HDMECs were re-suspended in the EBM-2 medium containing 0.1% FBS and seeded in triplicate into the coated plates at 2×10^4 cells/well. After a 6-h incubation, the cells were fixed and pictures were captured using LAS X. Tube-formation quantification was carried out using the Angiogenesis Analyzer function in ImageJ. For the knockdown study, HDMECs were transfected with negative control (NC) small interfering RNA (siRNA) and RAB17 siRNA for 48 h, followed by Matrigel tube-formation assays performed in the same manner.

RNA sequencing and differentially expressed genes analysis

Total RNA was extracted from both the control and DFU groups of HDMECs at passage 3 using TRIzol reagent (ThermoFisher, Waltham, MA, USA). RNA sequencing and preliminary analysis were conducted by OE Biotech Co., Ltd (Shanghai, China). Differentially expressed genes (DEGs) analysis was performed using the DESeq2 R package [22]. Significantly differentially expressed genes were identified using thresholds of *p*-value <0.05 and fold-change (FC) > 2

or FC < 0.5. To further analyse DEGs, gene set enrichment analysis (GSEA)_GO enrichment and GSEA_KEGG pathway (where KEGG is the Kyoto Encyclopedia of Genes and Genomes) enrichment analysis were conducted using the clusterProfiler R package based on the hypergeometric distribution [23].

Enrichment analysis

Hallmark gene sets were obtained from the Molecular Signature Database (http://gsea-msigdb.org) and employed as the background gene sets for both fast gene set enrichment analysis (fGSEA) and gene set variation analysis (GSVA). The Fgsea R package was used for computation of the enrichment scores between groups [24]. The GSVA R package was used to estimate the enrichment scores of each sample [25]. Finally, the limma R package was used to determine the *p* values [26]. Statistical significance was defined as *p*-value < 0.05.

scRNA-Seg data sources and processing

scRNA-seq data of individuals with human DFU and healthy subjects without diabetes mellitus were obtained from the Gene Expression Omnibus database under the accession number GSE165816. The Seurat R package was used for the majority analysis of scRNA-seq data [27], and 14 DFU samples and 11 control samples were extracted from the raw data and subjected to the creation of the Seurat objects. Following the quality control of genes (expressed in >3cells), cells (number of expressed genes to be between 200 and 2500) and mitochondrial genes (set to be <50%), the SCTransform algorithm was implemented for the data. The Seurat objects were then normalized, and highly variable genes were calculated, while scaling and removing technical variations. The Seurat objects were then integrated using the IntegrateData command. For dimensional reduction, principal component analysis and t-stochastic neighboring embedding (tSNE) methods were performed on the highly variable genes. Unsupervised clustering of cells was carried out using the FindClusters command with a resolution of 1.0. The clusters were annotated into 12 different cell types based on well-established cell-specific markers. HDMECs were isolated from the data and subjected to subclusters identification. DEGs analysis was conducted using a pseudobulk DESeq2-LRT method in the Libra R package [28].

Weighted gene correlation network analysis

Weighted gene correlation network analysis (WGCNA) was conducted using the WGCNA R package [29]. To generate an unsigned correlation matrix, the scale data of HDMECs scRNA-seq data were extracted from the complete scRNA-seq dataset. Subsequently, network topology was analysed using the pickSoftThreshold command, with a soft-threshold power estimated at 1. Modules were obtained using the blockwiseModules command, with the minimum size of modules set to 50 genes. The correlation between modules and phenotypes (DFU and control) was further analysed. Module

genes that exhibited the strongest correlation with DFU-HDMECs were extracted.

Least absolute shrinkage and selection operator regression

The intersection of DEGs obtained from our RNA-seq data and module genes exhibiting the strongest correlation with DFU-HDMECs in the scRNA-seq data were used to fit least absolute shrinkage and selection operator (LASSO) models through the glmnet R package [30]. The scale data of HDMECs scRNA-seq data were used as the training set, while our bulk RNA-seq data were employed as the validation set. After 10-fold cross-validation, lamda.min was selected as the estimated shrinkage variable. The validity of the model was assessed by drawing receiver operating characteristic (ROC) curves and calculating their corresponding area under the curve (AUC) values using the pROC package [31].

Immunohistochemistry

Skin samples from both humans and mice were paraformaldehyde-fixed, paraffin-embedded, sliced and stained. Immunohistochemistry staining was performed using an anti-RAB17 antibody (1 : 200, Zenbio, Chengdu, China) and incubated overnight at 4°C. The sections were then washed three times, incubated with horseradish peroxidase-conjugated secondary antibody, coloured with diaminobenzidine and counterstained with hematoxylin.

Cell transfection

HDMECs were seeded in 6-well plates and cultured to 80% confluence. siRNA targeting RAB17 (si-RAB17-1, si-RAB17-2) and scrambled negative control (si-NC) were procured from RiboBio (Guangzhou, Guangdong, China). Transfection was carried out with 50 nM (final concentration) si-RAB17-1, si-RAB17-2 or si-NC using Lipofectamine 3000 (Invitrogen, Carlsbad, CA, USA) for 48 h, following the manufacturer's protocol. RAB17-overexpressing lentivirus and the control lentivirus were developed by OBiO (Shanghai, China). Lentivirus infection was performed at a multiplicity of infection of 20 for 72 h. Subsequent experiments for qPCR, western blot or Matrigel tube-formation assay were performed as described above to measure the transfection efficiency and the effect of RAB17 on angiogenesis. For rescue experiments, ERK inhibitor (PD98059, Selleck) was added together with the lentivirus infection at a final concentration of 20 μ M.

Statistical analysis

The normality of the data was assessed using the Shapiro-Wilk test. Data that adhered to a normal distribution were expressed as mean ± standard deviation (SD). Otherwise, the data were represented by the median with its range. Statistical analyses were performed using the R software (v4.1.0, www.R-project.org) or GraphPad Prism version 8 (GraphPad Software, Inc). Student's t-test (two groups) or analysis of variance (ANOVA, three

or more groups, Bonferroni *post-hoc* test) was utilized to determine significant differences among groups when the data were normally distributed (*p*-value > 0.05, Kolmogorov–Smirnov test). For data that failed to meet the criteria of normal distribution, we employed the Mann–Whitney U test (two groups) or Kruskal–Wallis test (three or more groups, Dunn's *post hoc* test). A two-way ANOVA was used to compare data at multiple time points. *P*-values < 0.05 were regarded as significant.

Results

Characterization of CD31 MACS+ cells as ECs

The isolated MACS+ cells exhibited typical cobblestone shapes under a phase-contrast microscope (Figure 1a). Flow cytometry revealed that the purity of MACS⁺ cells was >95%, based on the expression of both CDH5 and CD31 (Figure 1b). Figure S1 shows gating strategies for the positively and negatively selected cells. The qPCR and western blotting results demonstrated that MACS+ cells expressed high levels of endothelial cell markers (CD31, CDH5 and vWF) while expressing low levels of α -SMA (Figure 1c, d). Furthermore, immunofluorescence staining indicated that the MACS+ cells expressed EC markers, including CD31, CDH5 and vWF, but not the smooth muscle cell (SMC) marker α -SMA (Figure 1e). Conversely, the HUASMCs displayed the opposite results (Figure 1e). Collectively, these findings suggest that the MACS+ cells possess characteristic features of ECs.

Impaired tube-formation capacity of DFU-HDMECs

While the changes in HUVECs cultured in hyperglycaemic media have been extensively studied [32], the phenotypes of DFU patient-derived HDMECs have not yet been explored. We aimed to investigate the phenotypic differences between Nor-HDMECs and DFU patient-derived HDMECs (DFU-HDMECs). To this end, we assessed the cell proliferation rates and migration abilities of Nor-HDMECs and DFU-HDMECs using cell counting (Figure 2a), EdU staining (Figure 2b, c), wound healing and transwell assays (Figure 2d-g). Unexpectedly, we found no significant differences in proliferation and migration rates between the two groups. In contrast, the Matrigel tube-formation assay demonstrated a significantly impaired angiogenesis capacity of DFU-HDMECs, based on the tube length and node number (Figure 2h, i). Given their association with diabetes-impaired angiogenesis [16,17], we also assessed the expression of HIF-1 α and VEGF-A between the two groups. qPCR and western blot results indicated a remarkable decrease in the expression of HIF-1 α and VEGF-A in DFU-HDMECs compared to that in Nor-HDMECs (Figure 2j, k). These results suggest that DFU-HDMECs have a significantly impaired capacity for angiogenesis.

Bulk-seq elucidates impaired angiogenesis in DFU-HDMECs

After demonstrating impaired angiogenesis in DFU-HDMECs, we conducted RNA-seq to screen angiogenesis-related

genes. We identified 147 DEGs between the patient groups, of which 138 were downregulated and 9 upregulated (Figure 3a, b). GSEA was then performed to assess the differences in biological processes (BPs) between DFUand Nor-HDMECs. GSEA revealed significant negative enrichment of angiogenesis (normalized enrichment score (NES) = -1.387389; adjusted p-value (p-adj) = 0.022) and endothelium development (NES = -1.65372; p-adj = 0.0099) in DFU-HDMECs (Figure 3c). Additionally, we identified other negatively enriched BPs, including oxidative phosphorylation, ATP synthesis coupled electron transport, aerobic electron transport chain and mitochondrial respiratory chain complex assembly (Figure S2a, see online supplementary material). Furthermore, molecular functions such as NAD(P)H dehydrogenase (quinone) activity and structural constituents of ribosomes (Figure S2b, see online supplementary material) as well as cellular components, including mitochondrial protein-containing complex, respirasome and inner mitochondrial membrane protein complex (Figure \$2c, see online supplementary material), were also identified. KEGG analysis showed significant enrichment of the VEGF signalling pathway, mitogen-activated protein kinase (MAPK) signalling pathway and oxidative phosphorylation (Figure S2d, see online supplementary material). These results support our in vitro findings and suggest the potential mitochondrial dysfunction of DFU-HDMECs.

We further confirmed our GSEA results by performing gene set variation analysis (GSVA) and fGSEA using hall-mark gene sets from MSigDB. GSVA revealed significant variations in angiogenesis (p-adj = 0.049), TNF- α signalling via NF- κ B (p-adj = 0.049) and the inflammatory response (p-adj = 0.049), with the highest absolute value of t observed for angiogenesis (t = -4.15; Figure 3d). Additionally, fGSEA showed a significant negative enrichment of angiogenesis (NES = -1.64; p-adj = 0.026) in DFU-HDMECs (Figure 3e). Collectively, these functional enrichment results validate the impairment of angiogenesis in DFU-HDMECs.

scRNA-seq confirms impaired angiogenesis in DFU-HDMECs

To elucidate the changes in DFU-HDMECs at the singlecell level, we performed scRNA-seq analysis using dataset GSE165816. Quality control, SCTransform, dimensionality reduction, clustering and cell annotations were carried out using the R package Seurat (v 4.1.1). A total of 63,190 cells passed quality control (Figure S3a-h, see online supplementary material); those with variations in the percentage of mitochondrial genes and differences in cell cycles were excluded from the analysis (Figure S3i-k, see online supplementary material). Using the t-distributed stochastic neighbour embedding (t-SNE) dimensionality reduction and K nearest neighbour methods, we identified 28 clusters (Figure S31, see online supplementary material), which were categorized into 12 known cell types based on cell-specific marker genes (Figure 4a, b) [33,34], and calculated the proportions of each cell type. Unexpectedly, the DFUs showed slightly higher proportions of HDMECs than the healthy controls, although

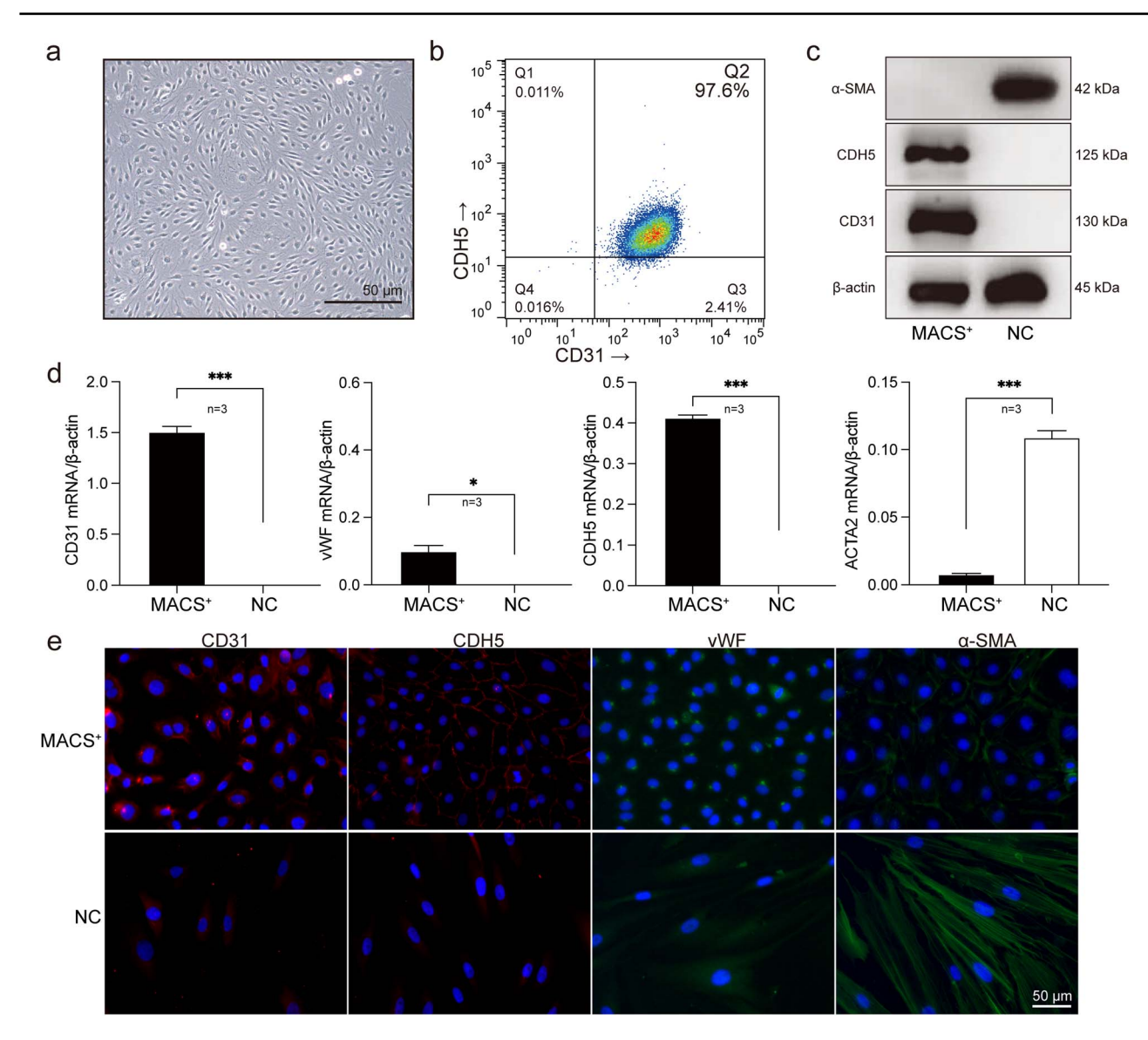


Figure 1. Patient-derived HDMECs showed typical characteristics of endothelial cells. (a) Bright-field microscopy showed typical cobblestone-like morphological features of patient-derived HDMECs (scale bar: $50 \mu m$). (b) Flow cytometric analysis detecting the positive rates of EC-specific markers CD31 and CDH5 in MACS⁺ cells. (c) Western blotting showing EC markers and SMC markers in MACS⁺ cells and NC cells. (d) mRNA levels of EC markers and SMC markers in MACS⁺ cells and NC cells measured by q-PCR. (e) Immunofluorescent staining showing the expression of EC markers and SMC markers in MACS⁺ cells and NC cells (Scale bar: $50 \mu m$). The data represent the mean \pm SD; *p < 0.05, , ***p < 0.05, , ***p < 0.001. HDMECs human dermal microvascular endothelial cells, MACS magnetic-activated cell sorting, EC endothelial cell, NC negative control, SMC smooth muscle cells, CDH5, cadherin 5, α -SMA actin alpha 2 smooth muscle, vWF Von Willebrand Factor, SD standard deviation

the difference was not significant (p = 0.9; Figure 4c). This result suggests that impaired angiogenesis may be the result of reduced tube-formation function rather than cell number.

To investigate the functional changes in HDMECs, we compared the results of bulk-seq and scRNA-seq analysis. HDMECs were isolated from the total cells and subjected to differential gene expression analysis using the pseudobulk method [28]. We isolated 2101 Nor-HDMECs and 2859 DFU-HDMECs, which were categorized into eight subclusters (Figure 4d, e). The proportion of cells in subclusters 7 and 3 was decreased and increased, respectively, in DFU-HDMECs compared to that in Nor-HDMECs (Figure 4f).

Through volcano plot and heatmap analyses, we identified 326 DEGs (Figure S4a, b, see online supplementary material). Notably, GSEA results showed significant negative enrichment of angiogenesis (NES = -1.644647; p-adj < 0.001) and wound healing (NES = -1.639841; p-adj < 0.001) in DFU-HDMECs (Figure 4g). We also observed the significant negative enrichment of other BPs, including phagocytosis, regulation of leukocyte activation and positive regulation of immune response (Figure S4c, see online supplementary material); molecular functions, including extracellular matrix structural constituent, glycosaminoglycan binding and extracellular matrix binding (Figure S4d, see online supplementary

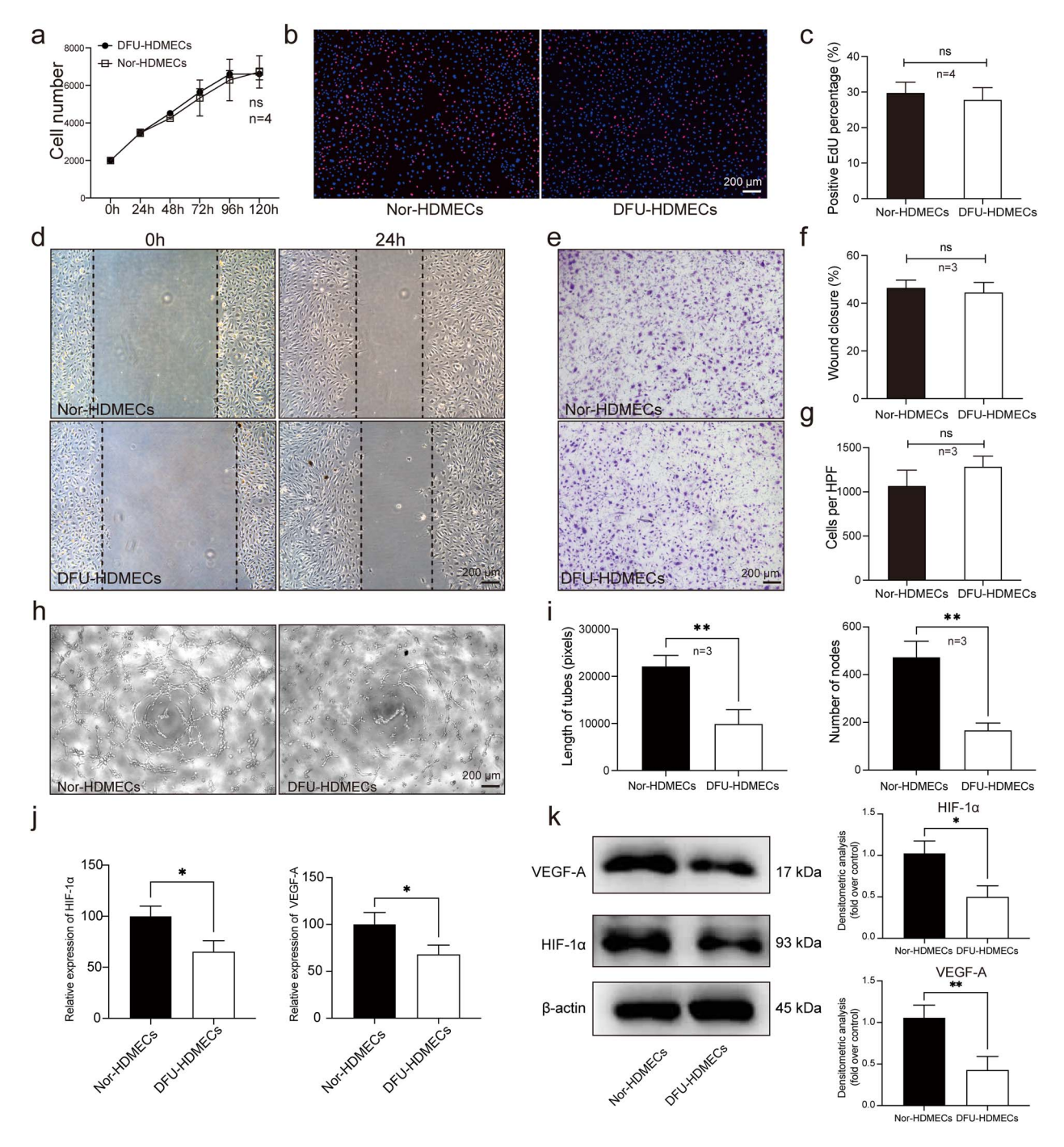


Figure 2. DFU-HDMECs showed impaired angiogenesis rather than proliferation and migration. (a) Cell counting assay for determining the proliferation of Nor-HDMECs and DFU-HDMECs. (b) EdU (red) proliferation assay and (c) quantitative analysis showing the positive rates of proliferating cells in Nor-HDMECs and DFU-HDMECs. Nuclei were stained blue by DAPI (scale bar: 200 μm). (d) Wound scratch assay images and (f) quantitative analysis for evaluation of the migration in monolayer of Nor-HDMECs and DFU-HDMECs (scale bar: 200 μm). (e) Transwell assay images and (g) quantitative analysis for evaluation of the migration through the membrane of Nor-HDMECs and DFU-HDMECs (scale bar: 200 μm). (h) Matrigel tube-formation assay showing the capillary-like structures of Nor-HDMECs and DFU-HDMECs (scale bar: 200 μm). (i) Quantitative analysis of tube formation using number of tubes and nodes. HIF-1α and VEGF-A expression levels in HDMECs between normal and DFU group were measured by (j) q-PCR and (k) western blotting. Results are represented as the mean ± SD; *p < 0.05, *p < 0.01; ns, not significant. DFU diabetic foot ulcer, Nor normal, HDMECs human dermal microvascular endothelial cells, EdU 5-ethynyl-2′-deoxyuridine, HIF-1α hypoxia inducible factor 1 subunit alpha, VEGF-A vascular endothelial growth factor A, SD standard deviation

material); and cellular components, including extracellular matrix, collagen-containing extracellular matrix and external encapsulating structure (Figure S4e, see online supplementary material). KEGG analysis revealed significant enrichment of

the advanced glycation end products (AGEs)/receptor for AGEs (RAGE) signalling pathway in diabetic complications (Figure S4f, see online supplementary material). GSVA analysis showed that only variations in angiogenesis were

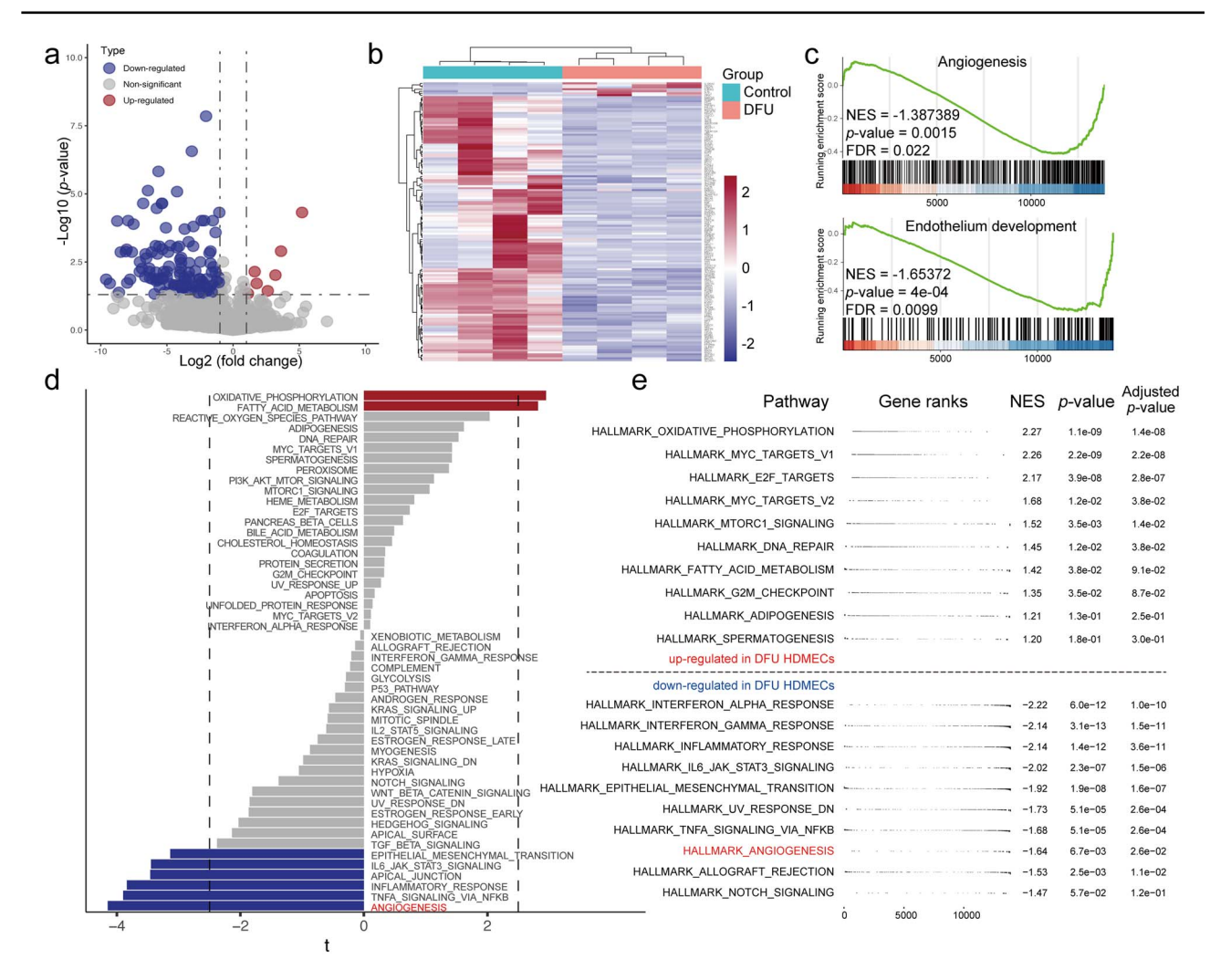


Figure 3. RNA sequencing and functional enrichment analysis showed impaired angiogenesis in DFU-HDMECs. (a) Volcano plot of genes differentially expressed between Nor-HDMECs and DFU-HDMECs. Up- or down-regulated genes are highlighted in red and blue respectively, whereas grey represents non-significant genes. (b) Heatmap of expressions of DEGs between Nor-HDMECs and DFU-HDMECs. (c) GSEA enrichment plots of the negatively enriched BP terms of angiogenesis and endothelium development in DFU-HDMECs compared to Nor-HDMECs. (d) The GSVA results showing the significantly up- or down-regulated hallmark gene sets in DFU-HDMECs compared to Nor-HDMECs. (e) The fGSEA plots of the significantly up- or down-regulated hallmark gene sets in DFU-HDMECs. A p-value <0.05 was considered statistically significant. DFU diabetic foot ulcer, Nor normal, HDMECs human dermal microvascular endothelial cells, DEGs differentially expressed genes, GSEA gene set enrichment analysis, GSVA gene set variation analysis, NES normalized enrichment score

statistically significant (p-adj = 0.017; Figure 4h). Similarly, fGSEA analysis identified the negative enrichment of angiogenesis (NES = -2.01; p-adj < 0.001; Figure 4i). These findings support the impairment of angiogenesis in DFU-HDMECs at the single-cell level.

Identification of RAB17 as a key gene via WGCNA and LASSO regression

We employed WGCNA to explore the key genes involved in the impairment of angiogenesis in DFU-HDMECs. Initially, we selected the top 2000 genes ranked by median absolute deviation and constructed a scale-free network after sample clustering and soft power threshold estimation (Figure S5a, b, see online supplementary material). We identified six co-expressed gene modules (Figure S5c, d, see online supplementary material), for which the eigengenes were

correlated to the clinical traits of DFU patients or healthy controls (Figure S6a, see online supplementary material). Among these, the blue (correlation = 0.18, p < 0.001) and turquoise (correlation = 0.21, p < 0.001) modules were found to be the most relevant in our study (Figure S6a, see online supplementary material).

We employed LASSO regression to identify relevant genes involved in the impairment of angiogenesis in DFU-HDMECs by calculating the intersection between DEGs in the bulk-seq data and module genes. scRNA-seq and bulk-seq data of HDMECs were used as the training and validation datasets, respectively. The LASSO model generated a λ value of 0.217, resulting in the identification of two genes, namely *RAB17* and *CD200*, with non-zero coefficients (Figure S6b, see online supplementary material). The gene signature prediction score showed significant

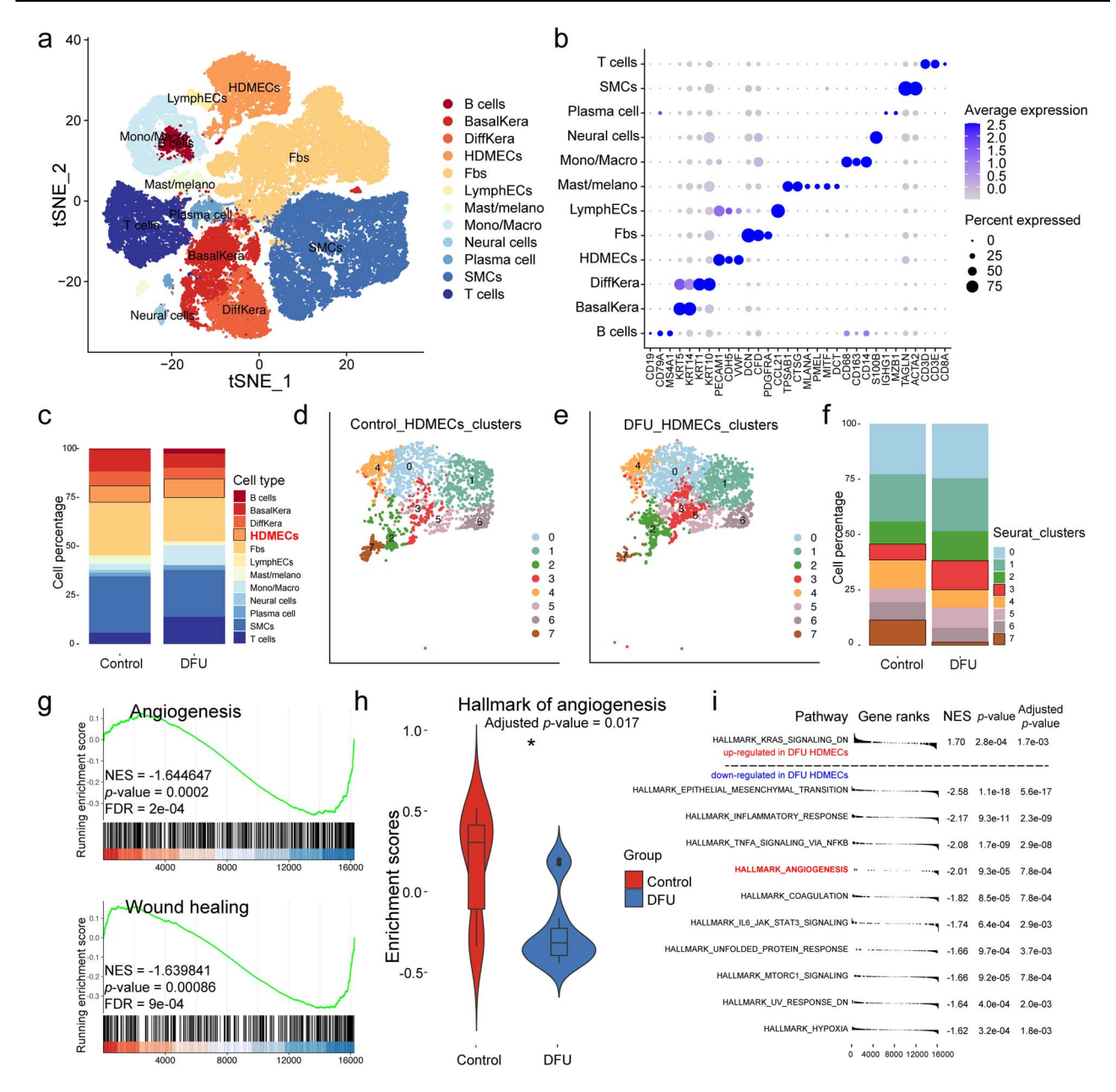


Figure 4. Single-cell RNA-seq reveals heterogeneity and impaired angiogenesis in HDMECs of DFU and normal skins. (a) t-SNE dimensionality reduction plot of the dataset GSE165816 with 63,190 cells passed quality control. The cells are coloured by manually annotated cell types. (b) Dot plot of the expression of the well-accepted cell-specific marker genes used for annotations of cell types. The colour indicates averaged expression levels of the scaled genes, and the size represents percentage of the marker genes expressed. (c) Stacked bar plots of the proportions of different types of cells in normal and DFU skins. (d, e) Split t-SNE plots of the HDMECs split from the whole dataset, shown by groups, depicting eight sub-clusters of HDMECs. (f) Stacked bar plots of the proportions of sub-types of HDMECs in normal and DFU skins. (g) GSEA plots showing the selected biological processes that are significantly affected (p-adj < 0.01) in DFU-HDMECs of the single-cell dataset. (h) Violin plot of GSVA showing the statistically significant variations (p-adj < 0.05) in single-cell data of DFU-HDMECs. (i) fGSEA plots of the significantly up- or down-regulated (p-adj < 0.05) hallmark gene sets in DFU-HDMECs extracted from the scRNA-seq data. DFU diabetic foot ulcer, Nor normal, HDMECs human dermal microvascular endothelial cells, tSNE t-distributed stochastic neighbour embedding, GSEA gene set enrichment analysis, GSVA gene set variation analysis, scRNA-seq single-cell RNA sequencing, NES normalized enrichment score

differences between the DFU and control groups (Figure S6c, see online supplementary material). We confirmed the validity of the LASSO regression result via ROC curve analysis (AUC = 0.9286; Figure S6d, see online supplementary material). The corresponding highest Youden's J value was 0.766. The AUC values for RAB17 and CD200 were 0.8506

and 0.9221 (Figure S6d, see online supplementary material), and the corresponding highest Youden's J values were 0.656 and 0.747, respectively. Furthermore, we validated these results using the validation dataset (AUC = 1 for the model; Figure S6e, see online supplementary material). The corresponding highest Youden's J value was 1.000. The AUC

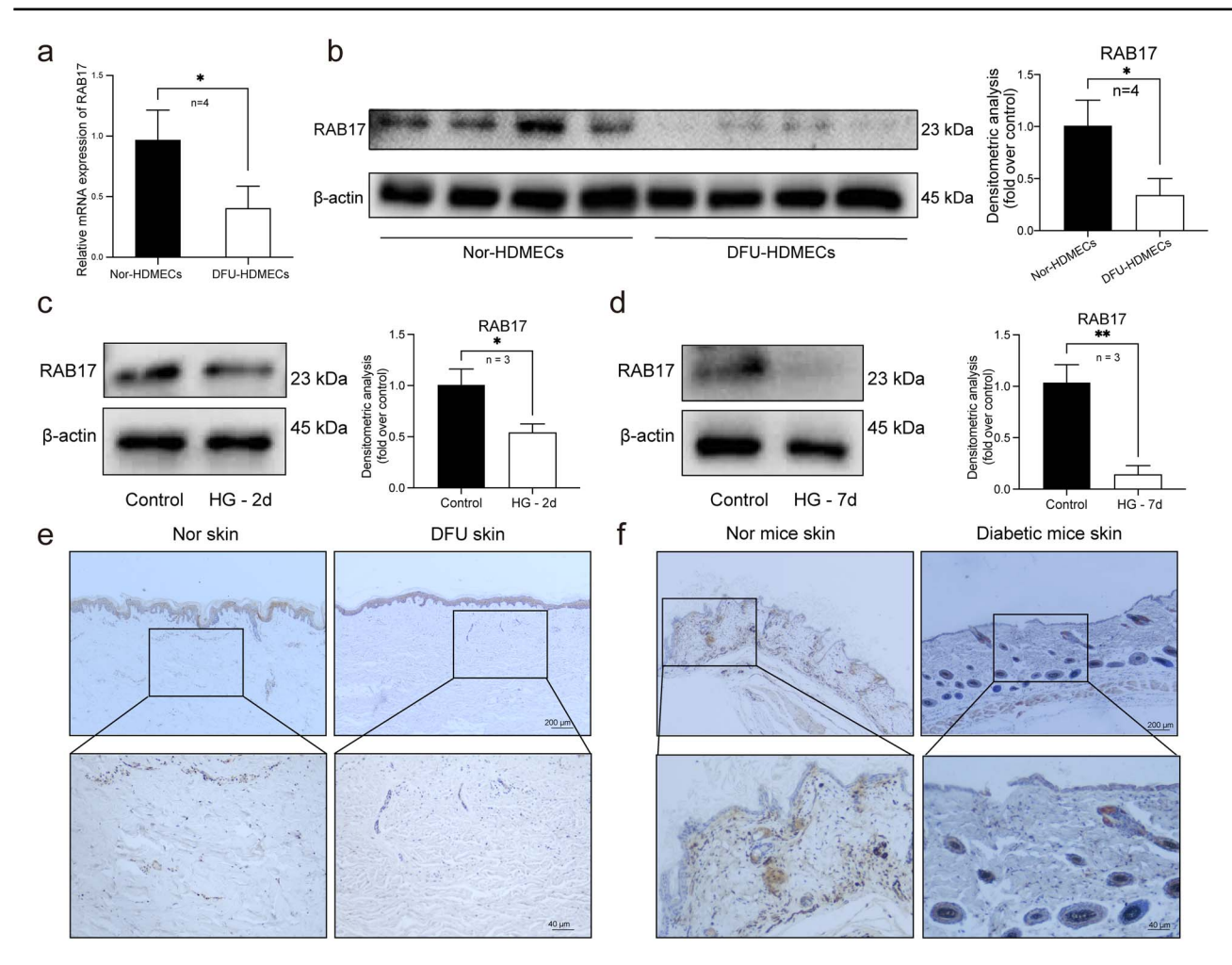


Figure 5. RAB17 level was decreased under hyperglycemic conditions. RAB17 expression level in HDMECs between normal and DFU group was measured by (a) q-PCR and (b) western blotting. (c, d) Western blotting assessing the expression of RAB17 in Nor-HDMEC exposed to high-glucose medium (30 mM D-glucose) for 2 and 7 days; 30 mM mannitol was used as an osmotic control. (e) Immunohistochemical analysis of RAB17 in the skin of normal patients and DFU subjects. Scale bar: 200 μ m (upper panel) and 40 μ m (lower panel) respectively. (f) Immunohistochemical analysis of RAB17 in the skin of normal mice and diabetic mice. Scale bar: 200 μ m (upper panel) and 40 μ m (lower panel) respectively. Results are represented as the mean \pm SD; *p < 0.05, **p < 0.01. DFU diabetic foot ulcer, Nor normal, HDMECs human dermal microvascular endothelial cells, HG high glucose, SD standard deviation

values for RAB17 and CD200 were 1 and 0.9375 (Figure S6f, see online supplementary material), and the corresponding highest Youden's J values were 1.000 and 0.750, respectively. These results suggest that the activity of RAB17 and CD200 might be associated with the phenotypic differences observed in DFU-HDMECs.

Downregulation of RAB17 in DFU-HDMECs

Based on the results of LASSO regression analysis, we examined the expression of key genes in HDMECs. The results of both single-cell and bulk sequencing analyses demonstrated a significant downregulation of the *RAB17* gene in DFU-HDMECs in contrast to that in Nor-HDMECs (Figure S7a, see online supplementary material) while the expression of CD200 showed an inconsistent trend (Figure S7e, f, see online supplementary material). To further explore the potential functions of RAB17 and CD200 in HDMECs, we conducted a functional enrichment analysis comparing RAB17+ with RAB17- and CD200+ with CD200- HDMECs. The GSEA

indicated positive enrichment of angiogenesis (NES = 1.977; p-adj = 0.028), blood vessel development (NES = 2.553; p-adj = 0.0002) and blood vessel morphogenesis (NES = 2.059; p-adj = 0.013) in RAB17⁺ HDMECs (Figure S7b, see online supplementary material). fGSEA also confirmed the positive correlation between RAB17 gene expression and angiogenesis (Figure S7c, see online supplementary material). In contrast, the GSEA results for CD200 did not reveal any significant enrichment of angiogenesis but instead showed an association with the regulation of cell communication, among other BPs (supplementary Figure S7g).

We explored the expression pattern of RAB17 in HDMECs using qPCR and western blotting. The results indicated reduced mRNA (Figure 5a) and protein levels (Figure 5b) of RAB17 in DFU-HDMECs compared to those in Nor-HDMECs. We investigated whether this decrease in RAB17 expression can be reproduced by exposing Nor-HDMECs to a hyperglycaemic environment. Western blotting showed a remarkable time-dependent decrease in

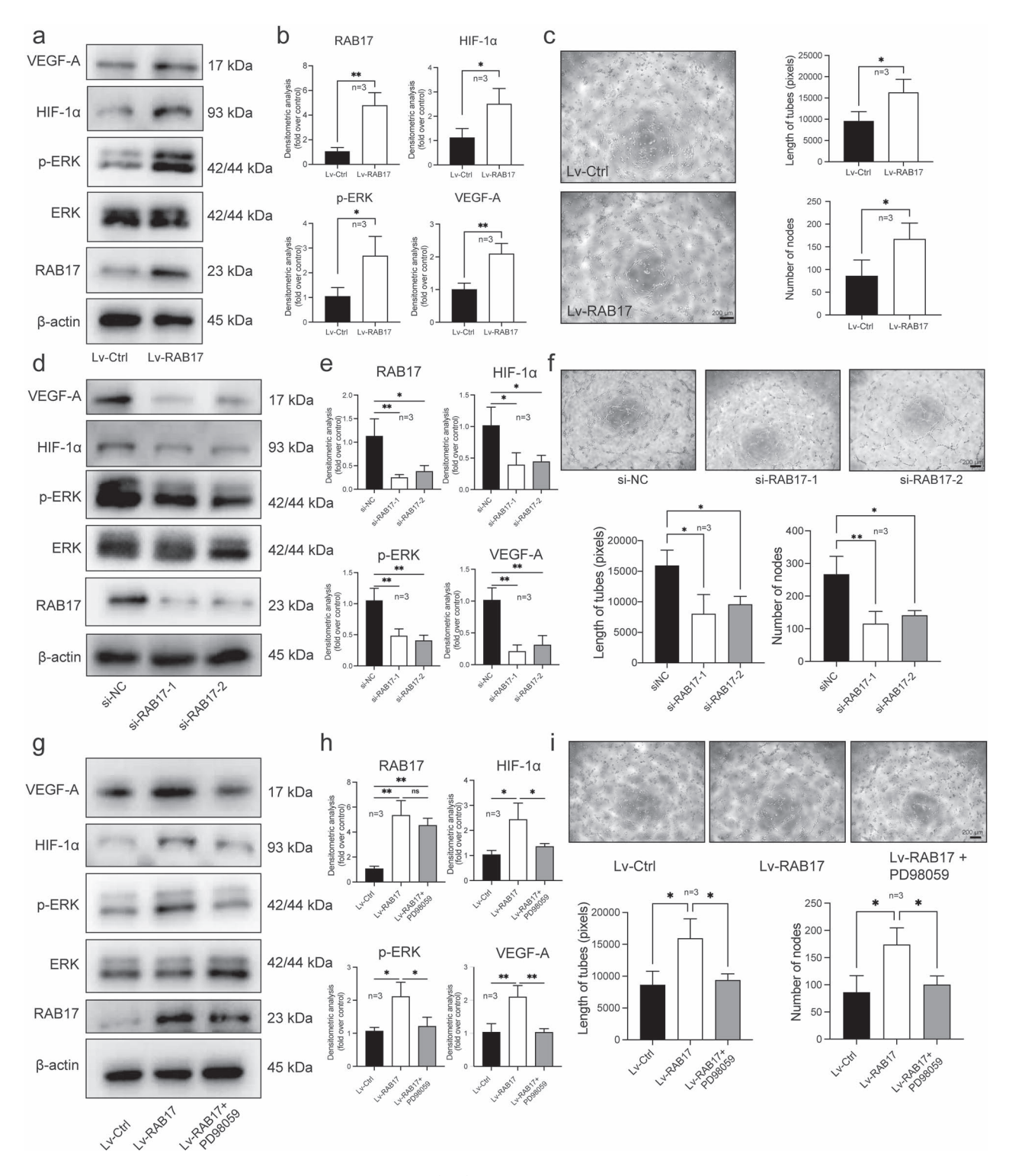


Figure 6. RAB17 affected angiogenic capacity of HDMECs *in vitro*. (a, b) Western blotting assessing the expression of RAB17 in DFU-HDMECs after RAB17-overexpressing lentivirus transfection, and the expressions of HIF-1α, VEGF-A, ERK and p-ERK in DFU-HDMECs after overexpression of RAB17. (c) Matrigel tube-formation assay of DFU-HDMECs following RAB17 overexpression and the quantitative analysis of tube formation using length of tubes and number of nodes. (d, e) Western blotting assessing the expressions of RAB17, HIF-1α, VEGF-A, ERK and p-ERK after knockdown by siRNA targeting RAB17. (f) Matrigel tube-formation assay and quantitative analysis of Nor-HDMECs following knock-down of RAB17. (g, h) Western blotting revealing the expression levels of HIF-1α, VEGF-A, ERK and p-ERK after overexpression of RAB17 with or without PD98059. (i) Matrigel tube-formation assay and quantitative analysis of DFU-HDMECs following RAB17 overexpression with or without PD98059. Results are represented as the mean ± SD; *p < 0.05, **p < 0.01. Lv lentivirus, Ctrl control, DFU diabetic foot ulcer, Nor normal, HDMECs human dermal microvascular endothelial cells, HIF-1α hypoxia inducible factor 1 subunit alpha, VEGF-A vascular endothelial growth factor A, si-RAB17 RAB17 small interfering RNA, si-NC negative control small interfering RNA, SD standard deviation

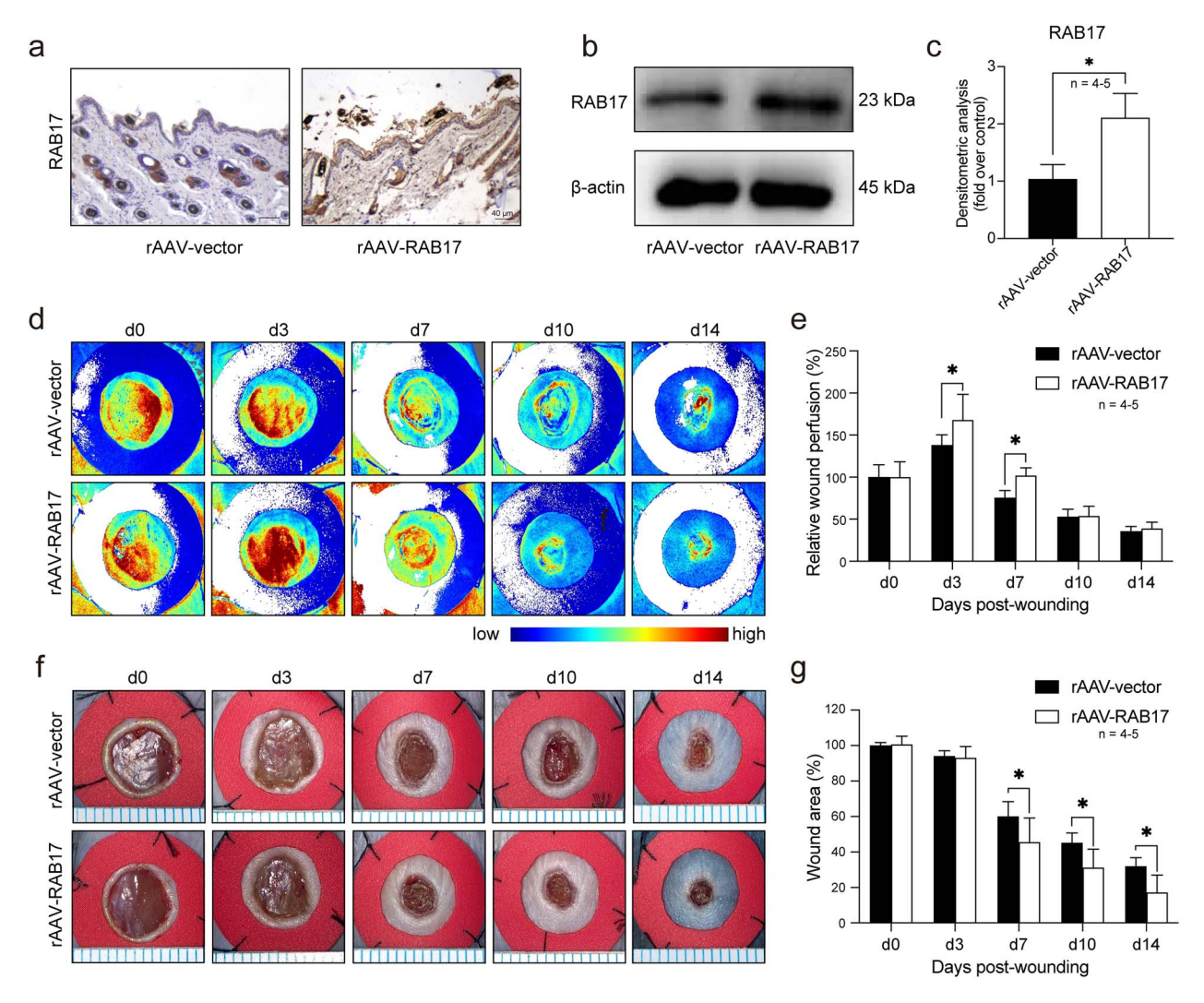


Figure 7. RAB17 overexpression promoted diabetic angiogenesis and wound healing in vivo. (a) Immunohistochemical analysis of RAB17 between groups after injection of rAAV-RAB17 or rAAV-vector. Scale bar: 40 μ m. (b, c) Western blotting assessing the expression of RAB17 in rAAV-RAB17 or rAAV-vector transfected mice skin. (d) Laser speckle contrast imager recording the wound perfusion images and (e) relative wound perfusion ratio in rAAV-RAB17 group and the control vector group; high- or low blood flow are represented in red and blue respectively. (f) Wound area monitored at the indicated days post-wounding and (g) quantitative analysis in rAAV-RAB17 group and the control vector group. Results are represented as the mean \pm SD; *p < 0.05. rAAV recombinant adenoassociated viral, SD standard deviation

the RAB17 expression of Nor-HDMECs under high-glucose conditions (Figure 5c, d). Additionally, we examined the expression of RAB17 in the dermal microvasculature of DFU patients using immunohistochemistry (Figure 5e); the results were consistent with the expression pattern observed in diabetic mouse skin (Figure 5f), displaying a significant decrease in RAB17 expression. Collectively, these findings suggest potential involvement of RAB17 in the regulation of angiogenesis in DFUs.

Effects of RAB17 expression manipulation on the angiogenic capacity of HDMECs

We investigated the role of RAB17 in DFU-HDMECs transfected with a RAB17-overexpressing lentivirus. Western blotting confirmed a significant increase in RAB17 expression by \sim 4-fold (Figure 6a, b). We first assessed the effect of RAB17 on the expression of HIF-1 α and VEGF-A, which were shown

to be downregulated in DFU-HDMECs (Figure 2j, k). Western blot results confirmed that the overexpression of RAB17 in DFU-HDMECs increased the expression of HIF-1 α and VEGF-A (Figure 6a, b). Moreover, overexpression of RAB17 significantly enhanced angiogenesis, as determined by the tube length and node number (Figure 6c). To further investigate the effect of RAB17 on angiogenesis, we knocked down RAB17 expression in Nor-HDMECs using siRNA. Results showed that that the expression of HIF-1 α and VEGF-A was significantly reduced (Figure 6d, e). Additionally, the Matrigel tube-formation assay revealed that angiogenesis was significantly impaired in RAB17-siRNA-transfected HDMECs, based on the tube length and node number (Figure 6f).

Furthermore, KEGG analysis revealed significant enrichment of the MAPK signalling pathway (Figure S7d, see online supplementary material). Considering that RAB17 is a member of the Ras superfamily, we hypothesised that a

regulatory relationship may exist between RAB17 and the MAPK/ERK signalling pathway. Western blotting showed that RAB17 overexpression induced the phosphorylation of ERK, whereas RAB17 silencing led to a significant decrease in ERK phosphorylation (Figure 6a, b, d, e). To evaluate whether the MAPK/ERK pathway is required for RAB17-mediated angiogenesis, we examined the effects of PD98059 [a MAPK/ERK kinase (MEK) inhibitor that inhibits the phosphorylation of ERK] on RAB17-induced ERK phosphorylation. Western blot analysis showed that treatment with PD98059 blocked the RAB17-induced phosphorylation of ERK (Figure 6g, h). Moreover, PD98059 treatment reversed the RAB17-mediated increase in HIF- 1α and VEGF-A expression (Figure 6g, h) and the RAB17mediated increase in angiogenesis (Figure 6i). Together, these results suggest that RAB17-mediated activation of the MAPK/ERK signalling pathway plays a crucial role in the regulation of angiogenesis in HDMECs.

Promotion of angiogenesis and wound healing in diabetic mice through RAB17 overexpression

Considering the promotion of angiogenesis in vitro by RAB17 overexpression in DFU-HDMECs, we conducted an assessment to determine whether RAB17 also promotes angiogenesis in vivo by wounding the STZ-induced diabetic mice. The mice received an intradermal dorsal injection of a RAB17overexpressing rAAV vector or a control vector. Immunohistochemistry and western blotting confirmed higher RAB17 expression in the rAAV-RAB17 group than in the control vector-infected mouse skin (Figure 7a-c). Using laser speckle imaging, we found that wound perfusion was significantly higher in the rAAV-RAB17 group than in the control vector group (Figure 7d, e). We compared the wound closure rate between the two groups to confirm the effects of RAB17 overexpression on wound healing. Wound images indicated a significant acceleration of wound closure in the rAAV-RAB17 group compared to that in the control group (Figure 7f, g). These findings suggest that RAB17 plays a role in promoting angiogenesis during diabetic wound repair in vivo.

Discussion

Angiogenesis plays a crucial role in the wound healing process, and vascular lesions have been extensively studied in the context of DFU pathology. Although abnormalities of the microvasculature of DFU include changes in capillary size and basement membrane structure, arteriolar occlusion is absent [35]. Although the microvessels are not occluded, blood flow distribution abnormality occurs in DFUs [36], implying functional defects in the newly formed microvessels. As HDMECs are the major components of microvessels, any functional changes in these cells can significantly impact DFU healing. Here, we isolated HDMECs from foot skin samples of DFU patients and found that these cells exhibit a significantly impaired capacity for angiogenesis, based on *in vitro*, bulk-seq and scRNA-seq results. This finding is

consistent with previous reports on diabetic patient-derived cells [37], indicating that HDMECs may lose their capacity for tube formation in the early stages of DFU formation. Surprisingly, our results showed no significant differences in proliferation or migration between the Nor-HDMECs and DFU-HDMECs, which is inconsistent with the characteristics of high glucose-stimulated HUVECs [32,38,39]. However, our findings align with those reported in diabetic patient skinderived cells [37]. These inconsistencies could be associated with the different sources of ECs used in the studies. Notably, HDMECs isolated from foreskin tissue are highly proliferative and poorly reflect the characteristics of those isolated from adult skin [40], which were used in our study and that of Vorwald et al. [37]. Additionally, clear differences have been reported between HUVECs and HDMECs, wherein factors that are pro-angiogenic on larger vessel-derived ECs such as HUVECs could be anti-angiogenic on HDMECs [41]. Another plausible explanation is that high-glucose treatments do not generate comparable models, especially since DFUs are generated by long-term simultaneous exposure to hyperglycaemia, hypoxia, chronic inflammation, oxidative stress and insulin resistance [42]. Thus, we consider that patient-derived HDMECs may provide a coherent and realistic characterization of their functioning in DFUs. Collectively, our results demonstrated that DFU-HDMECs exhibit poor angiogenic ability but no significant differences in proliferation or migration when compared to Nor-HDMECs.

Drawing on the broad perspective provided by the bulk-seq results, it was observed that DFU-HDMECs exhibited impaired angiogenesis, which was consistent with the changes observed in high-glucose-stimulated HDMECs [43]. Since growth factors are known to exert significant influence on the dynamics of diabetic wounds [3], we hypothesised that they might play a key role in determining the angiogenic ability of DFU-HDMECs. Indeed, our bulk-seq outcomes revealed modifications in the binding of growth factors, which were consistent with the sequencing results of diabetic patient-derived ECs [44] and high-glucose-induced ECs [45]. These results suggest that the altered binding of growth factors in ECs may contribute to their impaired angiogenic potential.

Growing evidence from single-cell transcriptome profiling indicates that EC functioning is tissue-specific in both humans [46] and mice [47]. Although the heterogeneity of dermal fibroblasts and immune cells in DFUs has been minutely investigated in a previous study, the characterization of HDMECs in the diabetic state was limited [33]. Interestingly, our results showed a slightly higher proportion of HDMECs in the DFU group than in the control group, although not statistically significant. One explanation could be attributed to biases in sample processing. Recent studies have shown that different dissociation strategies can lead to differences in the ratios of skin cells [48]. Single-nucleus sequencing could potentially solve this issue [49]. However, this could also be related to the unimpeded proliferation and migration of HDMECs in DFU tissues, which is consistent with our in vitro results. Moreover, the negative enrichment of angiogenesis based on the scRNA-seq data also validated our *in vitro* findings. As expected, the DEGs were partially different between the scRNA-seq and bulk-seq data, which could be due to the differences between sequencing methods [50]. The difference could also be the result of disparities in sex ratio and racial composition [51]. These results suggest that an integrated analysis could aid in determining the key genes related to DFUs.

Through the application of WGCNA and LASSO regression, we identified two genes associated with impaired angiogenesis in DFU-HDMECs, namely RAB17 and CD200. The use of WGCNA is based on the construction of a scalefree network that reflects the essential nature of the biological gene network [52] and has proven to be useful for the identification of disease-related genes in various contexts [53,54]. To our knowledge, however, no such work had been done on DFU-HDMECs. Key modules that were associated with the clinicopathological features of DFUs were identified through the WGCNA, and LASSO regression was performed to screen the most relevant variables [55]. Our results demonstrated that RAB17 expression was lower in DFU-HDMECs than in Nor-HDMECs; additionally, functional enrichment analysis showed that RAB17 was involved in angiogenesis. Conversely, CD200 exhibited opposing expression in the bulk-seq and scRNA-seq data, which may be attributable to the differences in cell sources. Enrichment analysis for CD200 did not demonstrate any enrichment of angiogenesisrelated terms. Therefore, we hypothesised that the downregulation of RAB17 expression could be associated with the impairment of angiogenesis in DFU-HDMECs. Nevertheless, CD200-expressing HDMECs might influence wound healing through other mechanisms, such as the regulation of tissue inflammation [56].

RAB17 is a small GTPase that belongs to the Rab family. The expression of RAB17 was initially reported to be specific to ECs [57], although it has recently been detected in melanocytes [58], hippocampal neurons [59] and macrophages [60], and cancer cells such as Hela [61], breast cancer [62], non-small cell lung cancer [19] and endometrial cancer cells [63]. RAB17 regulates basolateral to apical transcytosis and sustains polarized sorting [20], which is similar to polarization during tube formation, where ECs are polarized towards the basement membrane matrix [64]. However, the role of RAB17 in diabetic angiogenesis has remained unclear until now. Our results showed that RAB17 expression was reduced in DFU-HDMECs. Overexpression of RAB17 led to increased angiogenesis in vitro and in vivo. Furthermore, our results demonstrated that overexpression of RAB17 increased the expression of HIF- 1α and VEGF-A, which were rescued by inhibition of the MAPK/ERK signalling pathway. This is consistent with the results of previous studies showing that HIF-1 α upregulation promoted angiogenesis during diabetic wound repair [65,66]. In hepatocellular carcinoma, RAB17 silencing reduced phosphorylation of ERK (similar to our study) [18], while in non-small cell lung cancer, it increased the expression

of HIF-1 α and VEGF [19]. This inconsistency could be attributed to the differences between HDMECs and tumour cells or between diseases.

Some limitations of our study need to be acknowledged. We used rAAV to overexpress RAB17 in mice skin, which is insufficient for achieving EC-specific overexpression. In addition, more animal models are required for validation purposes.

Consistencies between our findings and those of previous studies provide auspicious directions for future investigations. During angiogenesis, one EC, typically tip cell, is selected to lead the adjacent ECs in the methodical formation of new blood vessels [67]. Tip cells extend filopodia to sense guidance cues, analogous to how neurons direct their movements [67]. This correspondence between the attributes of tip cells and the functions of RAB17 in filopodia formation of melanocytic cells [58] is intriguing. One potential explanation for this correlation is that RAB17 participates in the activation of blood vessel tip cells. In addition, RAB17 was previously found to be involved in bactericidal autophagosome formation and exosome secretion [61,68]. Earlier findings from our team demonstrated that autophagy deficiency in ECs accelerated wound healing in mice, possibly in a paracrinedependent fashion [69]. These observations further suggest that the reduced expression of RAB17 in DFU-HDMECs might influence the healing of DFUs through autophagy- or exosome-related pathways.

Conclusions

We observed a considerable impairment of angiogenesis in DFU-HDMECs through functional and bioinformatics analyses. Using scRNA-seq and bulk-seq, we identified RAB17 as a potential regulator of angiogenesis, with its expression being reduced in DFU-HDMECs. Overexpression of RAB17 enhanced angiogenesis as well as the expression of HIF-1 α and VEGF-A, partially through the MAPK/ERK signalling pathway *in vitro*. Additionally, *in vivo* experiments demonstrated that RAB17 overexpression promoted angiogenesis and diabetic wound healing. These findings suggest that RAB17 may serve as a promising target for attenuating impaired angiogenesis in diabetic wounds.

Abbreviations

AUC: Area under the curve; BPs: Biological processes; Bulk-seq: Bulk RNA sequencing; DEGs: Differentially expressed genes; DFUs: Diabetic foot ulcers; ECs: Endothelial cells; Edu: 5-Ethynyl-2'-deoxyuridine; FBS: Fetal bovine serum; GSEA: Gene set enrichment analysis; GSVA: Gene set variation analysis; fGSEA: fast gene set enrichment analysis; HDMECs: Human dermal microvascular endothelial cells; HIF-1 α : Hypoxia inducible factor-1 α ; HUVECs: human umbilical vein endothelial cells; HUASMCs: Human umbilical artery smooth muscle cells; KEGG: Kyoto Encyclopedia of Genes and Genomes; LASSO: Least absolute shrink and selection

operator; MACS: Magnetic-activated cell sorting; NES: Normalized enrichment score; MAPK/ERK: Mitogenactivated protein kinase/extracellular signal-regulated kinase; *p*-adj: Adjusted *p*-value; qPCR: Quantitative real-time PCR; rAAV: Recombinant adeno-associated viral; ROC: Receiver operating characteristics: scRNA-seq: Single-cell RNA-seq; siRNA: Small interfering RNA; α-SMA: Actin alpha 2 smooth muscle; SMC: Smooth muscle cell; STZ: Streptozotocin; tSNE: t-Distributed stochastic neighbour embedding; VEGF-A: Vascular endothelial growth factor A; vWF: von Willebrand Factor; WGCNA: Weighted gene co-expression network analysis.

Acknowledgements

We thank Dr Pei-Suen Tsou (University of Michigan Scleroderma Program) for help in isolating HDMECs, Dr Lan Zhang (Jinan University) for imaging assistance, Prof. Gexiu Liu, Miss Jingyi Gu and Mr Quan Yu (Jinan University) for their support in the lab. We thank Dr Zehua Li (Jinan University) and Miss Zhiqin Dong (Jinan University) for their help with the animal experiments.

Supplementary data

Supplementary data is available at Burns & Trauma Journal online.

Funding

This work was supported by National Nature and Science Foundation of P.R. China (No. 81871563, 82102345), the Medical Research Foundation of Guangdong Province (A2021165), the Fundamental Research Funds for the Central Universities (21619350), Guangdong Foundation for Basic and Applied Basic Research (2019A1515110161), Funding by Science and Technology Projects in Guangzhou (202201020002, 202201020004, 202201020468), the Clinical Frontier Technology Program of the First Affiliated Hospital of Jinan University, China (No. JNU1AF-CFTP-2022-a01231, No. JNU1AF-CFTP-2022-a01208) and Guangdong Provincial Key Areas R&D Programs (2022B1111080007).

Authors' contributions

HYD: conception and design, provision of study material, collection and/or assembly of data, data analysis and interpretation, and manuscript writing. SHL, JQL and XH: collection and/or assembly of data and data analysis and interpretation. LZT, XJ, JJL and XL: collection and/or assembly of data and data analysis and interpretation. TXC: conception and design, administrative support, data analysis and interpretation, and final approval of manuscript. YSH: conception and design, financial support, administrative support, data analysis and interpretation, and final approval of manuscript. HWL: conception and design, financial support, administrative support, data analysis, and interpretation and final approval of manuscript. All authors read and approved the final manuscript.

Ethics approval and consent to participate

The study was performed in accordance with the Declaration of Helsinki principles and was approved by the Medical Ethics Committee of the First Affiliated Hospital of Jinan University. Written informed patient consent was obtained from each patient. The animal experiment protocol was approved by the Laboratory Animal Ethics Committee of Jinan University and performed following institution guidelines.

Conflicts of interest

The authors declare that they have no conflicts of interest.

Data availability

The datasets used and/or analysed during this study are available from the corresponding author on reasonable request.

References

- Chen H, Cheng Y, Tian J, Yang P, Zhang X, Chen Y, et al. Dissolved oxygen from microalgae-gel patch promotes chronic wound healing in diabetes. Sci Adv. 2020;6:eaba4311. https:// doi.org/10.1126/sciadv.aba4311.
- 2. Fesseha BK, Abularrage CJ, Hines KF, Sherman R, Frost P, Langan S, *et al.* Association of Hemoglobin a(1c) and wound healing in diabetic foot ulcers. *Diabetes Care*. 2018;41:1478–85. https://doi.org/10.2337/dc17-1683.
- Okonkwo UA, DiPietro LA. Diabetes and wound angiogenesis. *Int J Mol Sci.* 2017;18. https://doi.org/10.3390/ijms18071419.
- Wu X, He W, Mu X, Liu Y, Deng J, Liu Y, et al. Macrophage polarization in diabetic wound healing. Burns. Dent Traumatol. 2022;10:tkac051. https://doi.org/10.1093/burnst/tkac051.
- Ishihara J, Ishihara A, Starke RD, Peghaire CR, Smith KE, McKinnon TAJ, et al. The heparin binding domain of von Willebrand factor binds to growth factors and promotes angiogenesis in wound healing. Blood. 2019;133:2559–69. https:// doi.org/10.1182/blood.2019000510.
- Cao XZ, Xie T, Lu SL. Receptor pathways of glycated basic fibroblast growth factor affecting the proliferation and vascularization of human dermal microvascular endothelial cells. *Chin j Burns*. 2021;37:17–24. https://doi.org/10.3760/cma.j. cn501120-20200916-00412.
- Bouïs D, Kusumanto Y, Meijer C, Mulder NH, Hospers GA. A review on pro- and anti-angiogenic factors as targets of clinical intervention. *Pharmacol Res.* 2006;53:89–103. https:// doi.org/10.1016/j.phrs.2005.10.006.
- Dixon D, Edmonds M. Managing diabetic foot ulcers: pharmacotherapy for wound healing. *Drugs*. 2021;81:29–56. https:// doi.org/10.1007/s40265-020-01415-8.
- Tsou PS, Campbell P, Amin MA, Coit P, Miller S, Fox DA, et al. Inhibition of EZH2 prevents fibrosis and restores normal angiogenesis in scleroderma. Proc Natl Acad Sci U S A. 2019;116:3695–702. https://doi.org/10.1073/pnas.1813006116.
- Fandaros M, Joseph K, Kaplan AP, Rubenstein DA, Ghebrehiwet B, Yin W. gC1qR antibody can modulate endothelial cell permeability in angioedema. *Inflammation*. 2022;45:116–28. https:// doi.org/10.1007/s10753-021-01532-w.
- 11. Peng L, Li Q, Wang H, Wu J, Li C, Liu Y, *et al.* Fn14 deficiency ameliorates psoriasis-like skin disease in a murine model. *Cell Death Dis.* 2018;9:801. https://doi.org/10.1038/s41419-018-0820-6.
- Lawley TJ, Kubota Y. Induction of morphologic differentiation of endothelial cells in culture. *J Invest Dermatol.* 1989;93:59s– 61. https://doi.org/10.1111/1523-1747.ep12581070.

- Clark PR, Manes TD, Pober JS, Kluger MS. Increased ICAM-1 expression causes endothelial cell leakiness, cytoskeletal reorganization and junctional alterations. *J Invest Dermatol*. 2007;127:762–74. https://doi.org/10.1038/sj.jid.5700670.
- Beckman JA, Doherty SP, Feldman ZB, Banks ES, Moslehi J, Jaffe IZ, et al. Comparative Transcriptomics of ex vivo, patientderived endothelial cells reveals novel pathways associated with type 2 diabetes mellitus. JACC Basic Transl Sci. 2019;4:567–74. https://doi.org/10.1016/j.jacbts.2019.05.012.
- 15. Singh K, Sinha M, Pal D, Tabasum S, Gnyawali SC, Khona D, et al. Cutaneous epithelial to mesenchymal transition activator ZEB1 regulates wound angiogenesis and closure in a Glycemic status-dependent manner. Diabetes. 2019;68:2175–90. https://doi.org/10.2337/db19-0202.
- Botusan IR, Sunkari VG, Savu O, Catrina AI, Grünler J, Lindberg S, et al. Stabilization of HIF-1alpha is critical to improve wound healing in diabetic mice. Proc Natl Acad Sci U S A. 2008;105:19426–31. https://doi.org/10.1073/pna s.0805230105.
- Rivard A, Silver M, Chen D, Kearney M, Magner M, Annex B, et al. Rescue of diabetes-related impairment of angiogenesis by intramuscular gene therapy with adeno-VEGF. Am J Pathol. 1999;154:355–63. https://doi.org/10.1016/s0002-9440 (10)65282-0.
- Qi J, Zhao P, Li F, Guo Y, Cui H, Liu A, et al. Down-regulation of Rab17 promotes tumourigenic properties of hepatocellular carcinoma cells via Erk pathway. Int J Clin Exp Pathol. 2015;8:4963–71.
- Wang M, Wang W, Ding J, Wang J, Zhang J. Down-regulation of Rab17 promotes cell proliferation and invasion in non-small cell lung cancer through STAT3/HIF-1α/VEGF signaling. *Thorac Cancer*. 2020;11:379–88. https://doi.org/10.1111/1759-7714.13278.
- 20. Striz AC, Tuma PL. The GTP-bound and Sumoylated form of the rab17 small molecular weight GTPase selectively binds Syntaxin 2 in polarized hepatic WIF-B cells. *J Biol Chem.* 2016;291:9721–32. https://doi.org/10.1074/jbc.M116.723353.
- 21. El-Remessy AB, Abou-Mohamed G, Caldwell RW, Caldwell RB. High glucose-induced tyrosine nitration in endothelial cells: role of eNOS uncoupling and aldose reductase activation. *Invest Ophthalmol Vis Sci.* 2003;44:3135–43. https://doi.org/10.1167/iovs.02-1022.
- 22. Love MI, Huber W, Anders S. Moderated estimation of fold change and dispersion for RNA-seq data with DESeq2. *Genome Biol.* 2014;15:550. https://doi.org/10.1186/s13059-014-0550-8.
- Yu G, Wang LG, Han Y, He QY. clusterProfiler: an R package for comparing biological themes among gene clusters. *OMICS*. 2012;16:284–7. https://doi.org/10.1089/omi.2011.0118.
- 24. Korotkevich G, Sukhov V, Budin N, Shpak B, Artyomov MN, Sergushichev A. Fast gene set enrichment analysis. *bioRxiv*. 2021;060012. https://doi.org/10.1101/060012.
- Hänzelmann S, Castelo R, Guinney J. GSVA: gene set variation analysis for microarray and RNA-seq data. BMC Bioinformatics. 2013;14:7. https://doi.org/10.1186/1471-2105-14-7.
- 26. Ritchie ME, Phipson B, Wu D, Hu Y, Law CW, Shi W, et al. Limma powers differential expression analyses for RNA-sequencing and microarray studies. *Nucleic Acids Res.* 2015;43:e47. https://doi.org/10.1093/nar/gkv007.
- 27. Hao Y, Hao S, Andersen-Nissen E, Mauck WM, 3rd, Zheng S, Butler A, et al. Integrated analysis of multimodal single-cell

- data. Cell. 2021;184:3573–87.e29. https://doi.org/10.1016/j.cell.2021.04.048.
- Squair JW, Gautier M, Kathe C, Anderson MA, James ND, Hutson TH, et al. Confronting false discoveries in single-cell differential expression. Nat Commun. 2021;12:5692. https:// doi.org/10.1038/s41467-021-25960-2.
- 29. Langfelder P, Horvath S. Fast R functions for robust correlations and hierarchical clustering. *J Stat Softw.* 2012;46:i11.
- Simon N, Friedman J, Hastie T, Tibshirani R. Regularization paths for Cox's proportional hazards model via coordinate descent. J Stat Softw. 2011;39:1–13. https://doi.org/10.18637/ iss.v039.i05.
- Robin X, Turck N, Hainard A, Tiberti N, Lisacek F, Sanchez JC, et al. pROC: an open-source package for R and S+ to analyze and compare ROC curves. BMC Bioinformatics. 2011;12:77. https://doi.org/10.1186/1471-2105-12-77.
- 32. Zhao J, Yang S, Shu B, Chen L, Yang R, Xu Y, *et al.* Transient high glucose causes persistent vascular dysfunction and delayed wound healing by the DNMT1-mediated Ang-1/NF-κB pathway. *J Invest Dermatol.* 2021;141:1573–84. https://doi.org/10.1016/j.jid.2020.10.023.
- Theocharidis G, Thomas BE, Sarkar D, Mumme HL, Pilcher WJR, Dwivedi B, et al. Single cell transcriptomic landscape of diabetic foot ulcers. Nat Commun. 2022;13:181. https://doi.org/10.1038/s41467-021-27801-8.
- 34. Shim J, Oh SJ, Yeo E, Park JH, Bae JH, Kim SH, et al. Integrated analysis of single-cell and spatial Transcriptomics in keloids: highlights on Fibrovascular interactions in keloid pathogenesis. J Invest Dermatol. 2022. https://doi.org/10.1016/ j.jid.2022.01.017.
- 35. LoGerfo FW, Coffman JD. Current concepts. Vascular and microvascular disease of the foot in diabetes. Implications for foot care. *N Engl J Med*. 1984;311:1615–9. https://doi.org/10.1056/nejm198412203112506.
- Falanga V. Wound healing and its impairment in the diabetic foot. *Lancet*. 2005;366:1736–43. https://doi.org/10.1016/s0140-6736(05)67700-8.
- Vorwald CE, Murphy KC, Leach JK. Restoring vasculogenic potential of endothelial cells from diabetic patients through spheroid formation. *Cell Mol Bioeng*. 2018;11:267–78. https:// doi.org/10.1007/s12195-018-0531-1.
- 38. Huang X, Sun J, Chen G, Niu C, Wang Y, Zhao C, *et al.* Resveratrol promotes diabetic wound healing via SIRT1-FOXO1-c-Myc Signaling pathway-mediated angiogenesis. *Front Pharmacol.* 2019;10:421. https://doi.org/10.3389/fphar.2019.00421.
- Chen C, Zhao C, Gu C, Cui X, Wu J. MiRNA-144-3p inhibits high glucose induced cell proliferation through suppressing FGF16. *Biosci Rep.* 2019;39. https://doi.org/10.1042/ bsr20181788.
- 40. Henrot P, Laurent P, Levionnois E, Leleu D, Pain C, Truchetet ME, et al. A method for isolating and culturing skin cells: application to endothelial cells, fibroblasts, keratinocytes, and melanocytes from punch biopsies in systemic sclerosis skin. Front Immunol. 2020;11:566607. https://doi.org/10.3389/fimmu.2020.566607.
- 41. Tsou PS, Amin MA, Campbell PL, Zakhem G, Balogh B, Edhayan G, et al. Activation of the thromboxane A2 receptor by 8-Isoprostane inhibits the pro-Angiogenic effect of vascular endothelial growth factor in scleroderma. *J Invest Dermatol*. 2015;135:3153–62. https://doi.org/10.1038/jid.2015.323.

- Hu SC, Lan CE. High-glucose environment disturbs the physiologic functions of keratinocytes: focusing on diabetic wound healing. *J Dermatol Sci.* 2016;84:121–7. https://doi.org/10.1016/j.jdermsci.2016.07.008.
- 43. Zhang S, Ke Z, Yang C, Zhou P, Jiang H, Chen L, et al. High glucose causes distinct expression patterns of primary human skin cells by RNA sequencing. Front Endocrinol (Lausanne). 2021;12:603645. https://doi.org/10.3389/fendo.2021.603645.
- 44. Wimmer RA, Leopoldi A, Aichinger M, Wick N, Hantusch B, Novatchkova M, *et al.* Human blood vessel organoids as a model of diabetic vasculopathy. *Nature*. 2019;565:505–10. https://doi.org/10.1038/s41586-018-0858-8.
- 45. Dong L, Zhang Z, Liu X, Wang Q, Hong Y, Li X, *et al.* RNA sequencing reveals BMP4 as a basis for the dual-target treatment of diabetic retinopathy. *J Mol Med (Berl)*. 2021;99:225–40. https://doi.org/10.1007/s00109-020-01995-8.
- Li Q, Zhu Z, Wang L, Lin Y, Fang H, Lei J, et al. Single-cell transcriptome profiling reveals vascular endothelial cell heterogeneity in human skin. *Theranostics*. 2021;11:6461–76. https:// doi.org/10.7150/thno.54917.
- Paik DT, Tian L, Williams IM, Rhee S, Zhang H, Liu C, et al. Single-cell RNA sequencing unveils unique transcriptomic signatures of organ-specific endothelial cells. Circulation. 2020;142:1848–62. https://doi.org/10.1161/circulationa ha.119.041433.
- 48. Rustagi Y, Abouhashem AS, Verma P, Verma SS, Hernandez E, Liu S, et al. Endothelial phospholipase Cγ2 improves outcomes of diabetic ischemic limb rescue following VEGF therapy. Diabetes. 2022;71:1149–65. https://doi.org/10.2337/db21-0830.
- 49. Ding J, Adiconis X, Simmons SK, Kowalczyk MS, Hession CC, Marjanovic ND, *et al.* Systematic comparison of single-cell and single-nucleus RNA-sequencing methods. *Nat Biotechnol*. 2020;38:737–46. https://doi.org/10.1038/s41587-020-0465-8.
- 50. Chung KB, Oh J, Roh WS, Kim TG, Kim DY. Core gene signatures of atopic dermatitis using public RNA-sequencing resources: comparison of bulk approach with single-cell approach. *J Invest Dermatol*. 2022;142:717–21.e5. https://doi.org/10.1016/j.jid.2021.07.169.
- 51. Luo Q, Chen Q, Wang W, Desrivières S, Quinlan EB, Jia T, et al. Association of a Schizophrenia-Risk Nonsynonymous Variant with putamen volume in adolescents: a Voxelwise and genomewide association study. *JAMA Psychiatry*. 2019;76:435–45. https://doi.org/10.1001/jamapsychiatry.2018.4126.
- Langfelder P, Horvath S. WGCNA: an R package for weighted correlation network analysis. BMC Bioinformatics. 2008;9:559. https://doi.org/10.1186/1471-2105-9-559.
- 53. Liu W, Huang X, Liang X, Zhou Y, Li H, Yu Q, et al. Identification of key modules and hub genes of keloids with weighted gene Coexpression network analysis. Plast Reconstr Surg. 2017;139:376–90. https://doi.org/10.1097/prs.000000000000000014.
- 54. Wang H, Zhou Z, Liu Y, Wang P, Chen L, Qi S, et al. Identification and validation of HOXD3 and UNC5C as molecular signatures in keloid based on weighted gene co-expression network analysis. Genomics. 2022;114:110403. https://doi.org/10.1016/j.ygeno.2022.110403.
- 55. Li Z, Huang B, Yi W, Wang F, Wei S, Yan H, *et al.* Identification of potential early diagnostic biomarkers of sepsis. *J Inflamm Res.* 2021;14:621–31. https://doi.org/10.2147/jir.S298604.

- Rütsche D, Michalak-Micka K, Zielinska D, Moll H, Moehrlen U, Biedermann T, et al. The role of CD200-CD200 receptor in human blood and lymphatic endothelial cells in the regulation of skin tissue inflammation. Cells. 2022;11. https://doi.org/10.3390/cells11061055.
- 57. Lütcke A, Jansson S, Parton RG, Chavrier P, Valencia A, Huber LA, et al. Rab17, a novel small GTPase, is specific for epithelial cells and is induced during cell polarization. J Cell Biol. 1993;121:553–64. https://doi.org/10.1083/jcb.121.3.553.
- Beaumont KA, Hamilton NA, Moores MT, Brown DL, Ohbayashi N, Cairncross O, et al. The recycling endosome protein Rab17 regulates melanocytic filopodia formation and melanosome trafficking. Traffic. 2011;12:627–43. https://doi.org/10.1111/j.1600-0854.2011.01172.x.
- Mori Y, Matsui T, Furutani Y, Yoshihara Y, Fukuda M. Small GTPase Rab17 regulates dendritic morphogenesis and postsynaptic development of hippocampal neurons. *J Biol Chem.* 2012;287:8963–73. https://doi.org/10.1074/jbc.M111.314385.
- Yin C, Kim Y, Argintaru D, Heit B. Rab17 mediates differential antigen sorting following efferocytosis and phagocytosis. *Cell Death Dis.* 2016;7:e2529. https://doi.org/10.1038/cddis.2016.431.
- 61. Haobam B, Nozawa T, Minowa-Nozawa A, Tanaka M, Oda S, Watanabe T, et al. Rab17-mediated recycling endosomes contribute to autophagosome formation in response to group a streptococcus invasion. Cell Microbiol. 2014;16:1806–21. https://doi.org/10.1111/cmi.12329.
- Diaz-Vera J, Palmer S, Hernandez-Fernaud JR, Dornier E, Mitchell LE, Macpherson I, et al. A proteomic approach to identify endosomal cargoes controlling cancer invasiveness. J Cell Sci. 2017;130:697–711. https://doi.org/10.1242/jcs.190835.
- 63. Zhou X, Xia G, Liu Y, Xin X, Shi R, An L, et al. Analysis of carcinogenic signaling networks in endometrial cancer identifies RAB17 as a potential target. J Cell Physiol. 2021;236:328–39. https://doi.org/10.1002/jcp.29845.
- 64. Arnaoutova I, George J, Kleinman HK, Benton G. The endothelial cell tube formation assay on basement membrane turns 20: state of the science and the art. *Angiogenesis*. 2009;12:267–74. https://doi.org/10.1007/s10456-009-9146-4.
- 65. Mace KA, Yu DH, Paydar KZ, Boudreau N, Young DM. Sustained expression of Hif-1alpha in the diabetic environment promotes angiogenesis and cutaneous wound repair. Wound Repair Regen. 2007;15:636–45. https://doi.org/10.1111/j.1524-475X.2007.00278.x.
- 66. Gao Y, Xie Z, Ho C, Wang J, Li Q, Zhang Y, et al. LRG1 promotes keratinocyte migration and wound repair through regulation of HIF-1α stability. J Invest Dermatol. 2020;140:455–64.e8. https://doi.org/10.1016/j.jid.2019.06.143.
- 67. Carmeliet P, Jain RK. Molecular mechanisms and clinical applications of angiogenesis. *Nature*. 2011;473:298–307. https://doi.org/10.1038/nature10144.
- Wu S, Luo M, To KKW, Zhang J, Su C, Zhang H, et al. Intercellular transfer of exosomal wild type EGFR triggers osimertinib resistance in non-small cell lung cancer. Mol Cancer. 2021;20:17. https://doi.org/10.1186/s12943-021-01307-9.
- 69. Li KC, Wang CH, Zou JJ, Qu C, Wang XL, Tian XS, *et al.* Loss of Atg7 in endothelial cells enhanced cutaneous wound healing in a mouse model. *J Surg Res.* 2020;249:145–55. https://doi.org/10.1016/j.jss.2019.12.004.